Rock Mech Rock Eng
DOI 10.1007/s00603-012-0252-z

ORIGINAL PAPER

Numerical Simulation of 3D Hydraulic Fracturing Based on an Improved Flow-Stress-Damage Model and a Parallel FEM Technique

L. C. Li · C. A. Tang · G. Li · S. Y. Wang · Z. Z. Liang · Y. B. Zhang

Received: 11 October 2011 / Accepted: 10 April 2012

Abstract The failure mechanism of hydraulic fractures in heterogeneous geological materials is an important topic in mining and petroleum engineering. A three-dimensional (3D) finite element model that considers the coupled effects of seepage, damage, and the stress field is introduced. This model is based on a previously developed two-dimensional (2D) version of the model (RFPA2D-Rock Failure Process Analysis). The RFPA3D-Parallel model is developed using a parallel finite element method with a message-passing interface library. The constitutive law of this model considers strength and stiffness degradation, stress-dependent permeability for the pre-peak stage, and deformation-dependent permeability for the post-peak stage. Using this model, 3D modelling of progressive failure and associated fluid flow in rock are conducted and used to investigate the hydro-mechanical response of rock samples at laboratory scale. The responses investigated are the axial stress–axial strain together with permeability evolution and fracture patterns at various stages of loading. Then, the hydraulic fracturing process inside a rock specimen is numerically simulated. Three coupled processes are considered: (1) mechanical deformation of the solid medium induced by the fluid pressure acting on the fracture surfaces and the rock skeleton, (2) fluid flow within the fracture, and (3) propagation of the fracture. The numerically simulated results show that the fractures from a vertical wellbore propagate in the maximum principal stress direction without branching, turning, and twisting in the case of a large difference in the magnitude of the far-field stresses. Otherwise, the fracture initiates in a non-preferred direction and plane then turns and twists during propagation to become aligned with the preferred direction and plane. This pattern of fracturing is common when the rock formation contains multiple layers with different material properties. In addition, local heterogeneity of the rock matrix and macro-scale stress fluctuations due to the variability of material properties can cause the branching, turning, and twisting of fractures.

Keywords Coupled fluid and solid deformation · Damage mechanics · Hydraulic fracture · Numerical stimulation · Fracture process · Heterogeneity

L. C. Li (✉) · C. A. Tang · G. Li · Z. Z. Liang · Y. B. Zhang
School of Civil Engineering, Dalian University of Technology, Dalian 116024, People's Republic of China
e-mail: li_lianchong@163.com

S. Y. Wang
Centre for Geotechnical and Materials Modelling, Civil, Surveying and Environmental Engineering, The University of Newcastle, Callaghan, NSW 2308, Australia

1 Introduction

Hydraulic fracturing occurs when fractures initiate and propagate as a result of hydraulic loading (i.e. pressure) applied by a fluid inside the fractures. The technique of hydraulic fracturing has been widely used in the petroleum engineering, mining, and geotechnical industries. For example, this technique is used to enhance the flow of fluids from oil, gas, and geothermal reservoirs in low-permeability formations (Economides and Nolte 2000). Other applications of hydraulic fracturing include the disposal of waste drill cuttings underground, heat production from geothermal reservoirs, goafing and fault reactivation in mining, and the measurement of in situ stresses (Adachi et al. 2007).

Mathematical modelling of the hydraulic fracturing process is usually performed to predict the response of fractures to the pumping rate while considering reservoir

Published online: 24 April 2012

and fluid properties and in situ stresses. Many researchers have studied hydraulic fracturing over the past several decades. Early efforts naturally focused on solutions for fractures with straight or penny-shaped geometry (Khristianovic and Zheltov 1955; Perkins and Kern 1961; Geertsma and de Klerk 1969; Nordren 1972). All of these solutions are approximate as they require assumptions about either the fracture opening or the pressure field. Such assumptions are necessary because of the difficulty in treatment of the complex fracture geometry growing under different stress and well conditions. However, these assumptions result in that the models in the studies cited above are not applicable to layered reservoirs where the fracture footprint is sensitive to changes in the confining stress across layer interfaces (Sousa et al. 1993; Savitski and Detournay 2002; Adachi et al. 2007).

In recent years, research has focused on the development of numerical algorithms to model the three-dimensional (3D) propagation of hydraulic fractures in layered strata characterised by different mechanical properties and/or in situ stresses. The main progress in these studies has been in the development of pseudo-three-dimensional fracture models (P3D model) and planar three-dimensional fracture models (PL3D model) (Simonson et al. 1978; Adachi et al. 2007). Incorporated with these proposed 2D and 3D models, research has focused on the modelling of hydraulic fractures, and many computer codes, including ENERFRAC, MFRAC, TRIFRAC, GOHFER, FRANC3D, and HYFRANC3D (Barree 1983; Vandamme and Curran 1989; Warpinski et al. 1993; Carter et al. 2000), have been developed. However, some issues concerning the modelling of hydraulic fractures should be further investigated. These issues include the following:

1. The true 3D or ''out of plane'' effects should be efficiently modelled. The success of fracture stimulation is largely dependent on the shape and propagation of the generated hydraulic fracture. A fracture initiating from a deviated wellbore is subjected to a complex stress state that leads to a development of the complex fracture geometry. The principles behind the reorientation of fractures remain poorly understood (Abass et al. 1992; Crosby et al. 1998; Mahrer 1999; Mofazzal Hossain and Rahman 2008). The visualisation of complex fracture growth in a non-preferred direction is important to understanding the physical reasons for increasing injection pressure and decreasing fracture volume. A recent trend has been, therefore, to develop coupled non-planar fracture models and to use them in parametric studies to understand complex fracture growth (Sousa et al. 1993; Dong and de Pater 2001; Siebrits and Peirce 2002; Rungamornrat et al. 2005; Zhang and Jeffrey 2006).
2. To improve the performance of hydraulic fracturing engineering projects, it is necessary to accurately predict the coupled behaviour of fluid flow and stress in fractured and fracturing rocks and particularly the effects due to damage (initiation, propagation and coalescence of fractures) in rock formation. Despite recent interest in coupling fluid flow and geomechanical deformation processes in a single model in which the interaction of flow and deformation (stress) can be modelled simultaneously, most hydraulic fracturing models remain uncoupled. However, in all hydraulic fracturing problems, there is a strong interaction between deformation (stress) and fluid flow. Standard modelling of hydraulic fracturing without considering this interaction can lead to significant errors (Yale et al. 2000; Susan et al. 2003; Garcia and Teufel 2005; Yuan and Harrison 2005).
3. With the advent of real-time micro-seismic, tiltmeter, and other monitoring techniques during hydraulic fracturing, there is a growing need for fast fully 3D models that can be used to update treatment designs in real time as information is fed back into the models. These updates are enabled through the use of 3D modelling based on high-performance computing (HPC). Over the past 20 years, HPC has become an affordable resource to researchers in the scientific community. The computational environment for solving geotechnical problems is transforming from single desktop PCs to HPC systems (Shah et al. 1997; Blaheta et al. 2006). Although there have been attempts to model fully 3D hydraulic fractures (Carter et al. 2000; Adachi et al. 2007; Lee and Ghassemi 2011), the computational burden of such coupled systems remains excessive. Even so, fully 3D models are essential in complex situations such as the oil/water contact within the pay zone layers and the intercalation of shale between the pay zone and adjacent layers. Fully 3D models are also important to the validation of P3D model (Legarth et al. 2005; Adachi et al. 2007).

As an increasing number of coupled non-planar fracture models are developed and used for hydraulic fracturing, this study investigated the non-planar hydraulic fracturing using a three-dimensional Rock Failure Process Analysis-Parallel (RFPA3D-Parallel) code. RFPA3D-Parallel is based on an improved flow-stress(strain)-damage (FSD) model (Tang 1997; Tang et al. 2002; Liang et al. 2004). The governing equations and the parallel FEM solution strategy in RFPA3D-Parallel were described and discussed. Then, a series of 3D numerical tests of the failure processes in rock specimens during hydraulic fracturing were performed with RFPA3D-Parallel running on a Lenovo 1800 HPC cluster system.

2 An Introduction to RFPA3D-Parallel

To investigate complex fracture growth in three dimensions, the numerical code RFPA3D-Parallel was developed. RFPA3D-Parallel is an extension of two-dimensional Rock Failure Process Analysis (RFPA2D) (Tang 1997; Tang et al. 2002). RFPA2D is a 2D finite element code that can simulate the fracture and failure process of quasi-brittle materials such as rock. RFPA2D has been successfully applied to 2D modelling of hydraulic fracturing, slope failure, and water outbursts in coal mining (Yang et al. 2004; Li et al. 2005, 2006, 2011a, b; Wang et al. 2009).

In RFPA3D-Parallel, the finite element method (FEM) is employed as the basic stress analysis tool, where the eight-node isoparametric element is used as the basic element in the finite element mesh. RFPA3D-Parallel was developed with the following assumptions:

- The rock mass is assumed to be fully saturated with fluid flow governed by Darcy's law. Additionally, the coupled process between stress/strain and fluid flow in the deforming rock mass is governed by Biot's consolidation theory (Biot 1941).
- The rock material at the elemental scale is assumed to be elasto-brittle with a residual strength. The mechanical behaviour of rock is described by an elastic damage constitutive law, and the residual strain/deformation upon unloading is not considered.
- An element is considered to fail in tensile mode when the minimum principal stress exceeds the tensile strength and fail in shear when the shear stress satisfies the Mohr–Coulomb failure criterion.
- The isotropic conditions are considered for the hydraulic behaviour at the elemental scale, i.e. the permeability of an element varies as a function of the stress state during elastic deformation and increases according to a deformation-dependent law when the element is damaged.
- The heterogeneity of rock materials is considered by assuming that the mechanical properties, such as Young's modulus and the strength properties, conform to the Weibull distribution (specified by the Weibull distribution parameters).

Because of grain-scale heterogeneity, the failure strength in a rock can vary significantly. To include the statistical variability of the bulk failure strength in RFPA3D-Parallel, the mechanical parameters of the model elements are assumed to follow a Weibull distribution:

$$f(u) = \frac{m}{u_0}\left(\frac{u}{u_0}\right)^{m-1}\exp\left(-\frac{u}{u_0}\right)^{m} \tag{1}$$

where u is the element parameter (such as Young's modulus, Poisson's ratio, or strength properties), u_0 is the scale parameter related to the average value of the element parameter, and m is the homogeneity index defining the shape of $f(u)$ representing the degree of homogeneity. A heterogeneous material can be numerically produced in a computer simulation by discretising with many elements, and each one is assumed to be isotropic and homogeneous.

2.1 Constitutive Laws

In this section, an improved flow-stress(strain)-damage (FSD) model is presented that explicitly represents a relationship between stress(strain), damage and permeability. In RFPA3D-Parallel, isotropic conditions are considered for the hydraulic behaviour at the elemental scale. According to Darcy's law of seepage flow in porous media, the flow of a fluid (water) is governed by

$$\nabla\left[\frac{k\rho_1 g}{\mu_1}(\nabla P - \rho_1 g \nabla Z)\right] = S\frac{\partial P}{\partial t} - \alpha\frac{\partial \varepsilon_v}{\partial t} \tag{2}$$

where k is permeability, ρ_1 is fluid density, μ_1 is fluid dynamic viscosity, g is gravity, P is pore fluid pressure, Z is elevation, S is storage coefficient, α is Biot's coefficient, and ε_v is volumetric strain.

The equilibrium equations and the strain–displacement relations can be expressed as

$$\frac{\partial \sigma_{ij}}{\partial x_{ij}} + f_i = 0 \quad (i,j = 1,2,3) \tag{3}$$

$$\varepsilon_{ij} = \frac{1}{2}(U_{i,j} + U_{j,i}) \tag{4}$$

where σ_{ij} is total stress in the ij-plane, f_i is volumetric body force, ε_{ij} is strain, and U_i is solid displacement. The governing equations for the elastic deformation of an isotropic linear poroelastic medium are

$$Gu_{i,jj} + \frac{G}{1-2v}u_{j,ji} - \alpha P_i + f_i = 0 \tag{5}$$

where G is shear modulus.

Initially, the element is considered to be elastic; its elastic properties can be defined by Young's modulus and Poisson's ratio. The stress–strain curve of each element is considered to be linear elastic until the given damage threshold is attained. As previously mentioned, we choose the maximum tensile stress (or strain) criterion and Mohr–Coulomb criterion as damage thresholds. The tensile stress (or strain) criterion is used first to determine whether an element is damaged. If the element is not damaged in tensile mode, the Mohr–Coulomb criterion is then used to determine whether the element is damaged in shear. The sign convention used throughout this paper is that compressive stresses and strains are positive. All following equations operate on effective stresses only.

In elastic damage mechanics, the elastic modulus may degrade gradually as damage progresses, and the elastic modulus of the damaged material is defined as

$$E = (1 - D)E_0 \tag{6}$$

where D is the damage variable and E_0 is the elastic modulus of the undamaged material. The element and its damage are assumed to be isotropic, and therefore, E, E_0 and D are all scalar. D ranges from zero (0.0) for the undamaged material to one (1.0) to represent full failure.

2.1.1 Damage Evolution of the Element in Tensional State

When the mesoscopic element is under uniaxial tension, the constitutive relationship illustrated in Fig. 1a is adopted. Figure 1a presents the elastic-brittle damage constitutive relations with given specific residual strength.

When the tensile stress in an element reaches the tensile strength f_t, i.e. $|\sigma_3| > f_t$, the damage variable D can be calculated as

$$D = \begin{cases} 0 & \varepsilon > \varepsilon_{t0} \\ 1 - \frac{f_{tr}}{\varepsilon E_0} & \varepsilon_{tu} < \varepsilon \le \varepsilon_{t0} \\ 1 & \varepsilon \le \varepsilon_{tu} \end{cases} \tag{7}$$

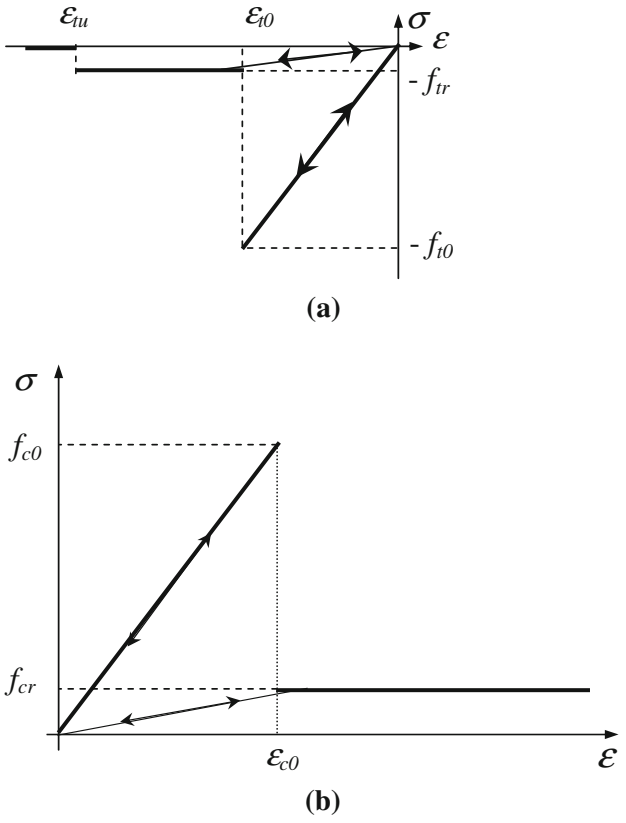

Fig. 1 Elastic-brittle damage constitutive law of element subject to uniaxial stress. **a** The case under uniaxial tensile stress, **b** the case under uniaxial compressive stress

where f_{tr} is the residual tensile strength, ε_{t0} is the strain at the elastic limit, which is the so-called threshold strain for tensile damage, while ε_{tu} is the ultimate tensile strain, at which the element would be completely damaged in tension as shown in Fig. 1a.

The generalised Hooke's law in the principal stress state can be expressed as

$$\sigma_i = \frac{E}{1+v}\left[\varepsilon_i + \frac{v}{1-2v}\varepsilon_{jj}\right] \quad (i,j = 1,2,3) \tag{8}$$

From Eq. 8 and the maximum tensile stress criterion, one may obtain

$$E = \frac{f_t}{\frac{\varepsilon_3}{1+v} + \eta\varepsilon_v} \tag{9}$$

where $\eta = \frac{v}{(1+v)(1-2v)}$.

From Eqs. 6 and 9, the damage variable D in the triaxial stress state can be defined as

$$D = 1 - \frac{f_t}{\frac{\varepsilon_3 E_0}{1+v} + \eta E_0 \varepsilon_v} \tag{10}$$

2.1.2 Damage Evolution of the Element in Compressive State

To describe the element damage under compressive or shear stress conditions, we use the Mohr–Coulomb criterion as the second damage criterion

$$\sigma_1 - \psi\sigma_3 \ge f_c \tag{11}$$

where f_c is the uniaxial compressive strength, $\psi = \frac{1+\sin\phi}{1-\sin\phi}$ and ϕ is the internal friction angle.

Corresponding to the damage evolution laws in tension, similar damage evolution laws are given in Fig. 1b when the element is under uniaxial compression and damaged in shear according to the Mohr–Coulomb criterion. The damage variable under uniaxial compression is described as

$$D = \begin{cases} 0 & \varepsilon < \varepsilon_{c0} \\ 1 - \frac{f_c}{\varepsilon E_0} & \varepsilon \ge \varepsilon_{c0} \end{cases} \tag{12}$$

When an element is under a triaxial stress state, from Eqs. 8 and 11, one can obtain

$$E = \frac{f_c}{\frac{\varepsilon_1}{1+v} + \eta\varepsilon_v - \left(\frac{\varepsilon_3}{1+v} + \eta\varepsilon_v\right)\psi} \tag{13}$$

Using Eqs. 6 and 13, the damage variable D in the triaxial stress state can be defined as

$$D = 1 - \frac{f_c}{E_0\left[\frac{\varepsilon_1}{1+v} + \eta\varepsilon_v - \left(\frac{\varepsilon_3}{1+v} + \eta\varepsilon_v\right)\psi\right]} \tag{14}$$

In this model, the element may gradually damage according to the above elastic damage constitutive

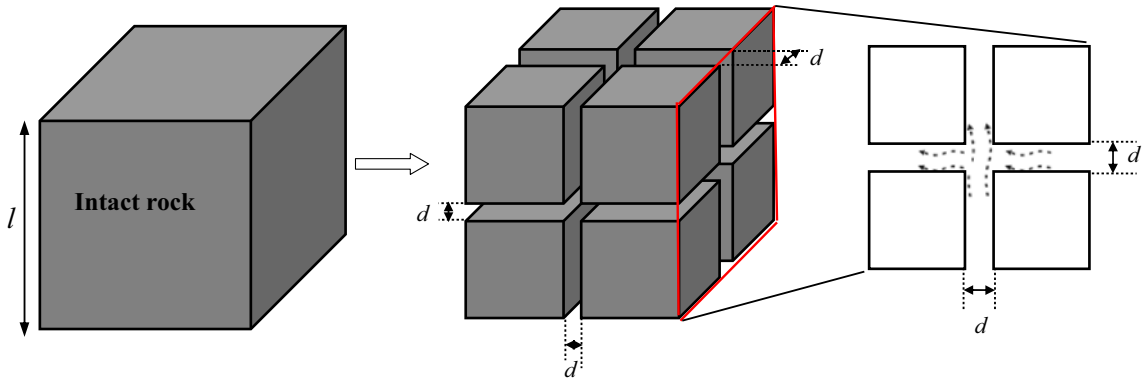

Fig. 2 Schematic illustration of permeability of a rock element due to brittle failure

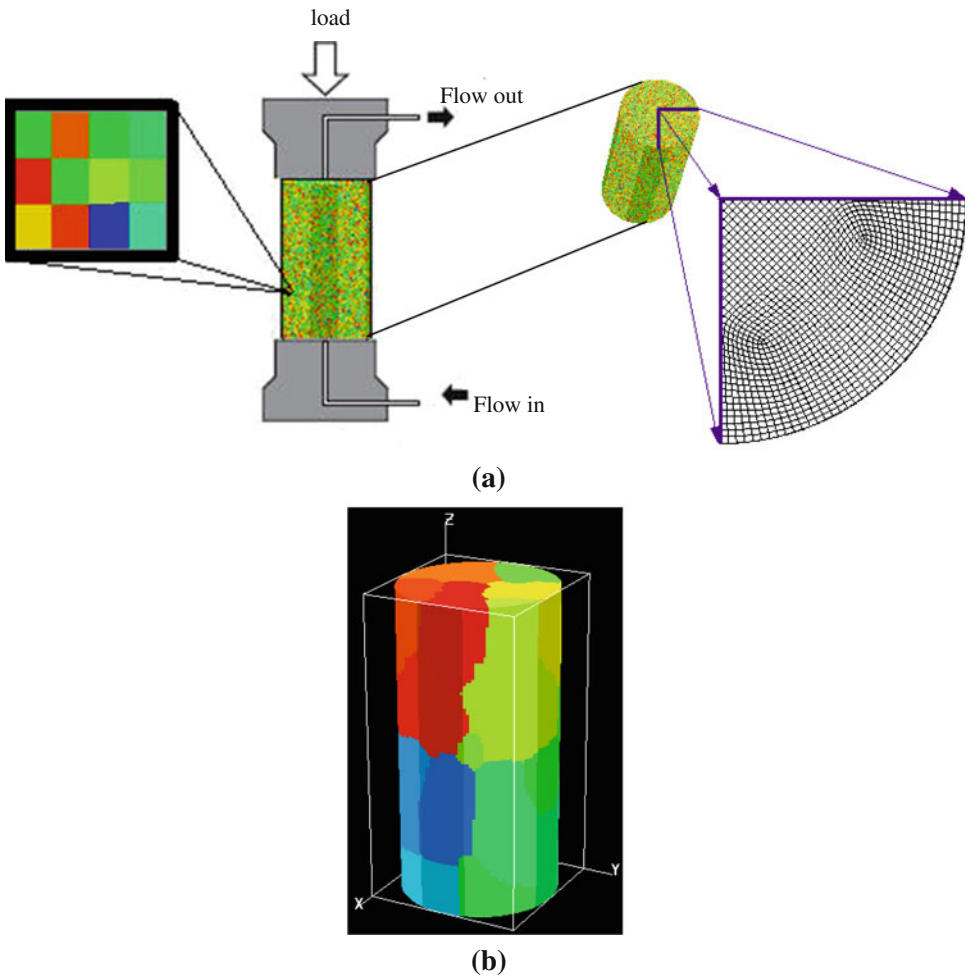

Fig. 3 Model setup for numerical simulation on the failure process of rock sample subject to hydro-mechanical loading: **a** sample configuration and meshes, **b** sub-domains for parallel FEM computation; each sub-domain contains 42,500 elements

relationship. Only elements whose ultimate tensile strain has been attained are displayed as cracks with black colour in the post-processing figures. Then the elastic modulus of cracked elements is specified to be a relatively small number, i.e. 1.0e−5. Both tensile damage and shear damage lead to the degradation of elements, but tensile damage is considered to be the direct cause of crack initiation. One of the main features of this type of model is that there is no need for a pre-existing crack to simulate the crack initiation and propagation. This approach to simulating cracks is similar to a smeared crack model, i.e. no special singular element is used, which has the advantage of leaving the mesh topology untouched. A similar principle has been addressed and applied to modelling concrete damage (Pietruszczak and Xu

Table 1 Rock properties of the sample

Parameters	Value	Unit
Homogeneity index (m)	2.0	
Young's modulus (E_0)	22	GPa
Compressive strength (f_c)	120	MPa
Poisson's ratio (v)	0.25	
Internal friction angle (ϕ)	30	°
Uniaxial tensional strength (f_t)	12	MPa
Permeability coefficient (k_0)	1e−8	cm/s
Coefficient of pore-water pressure (α)	0.8	
Coupling coefficient (β)	0.1	

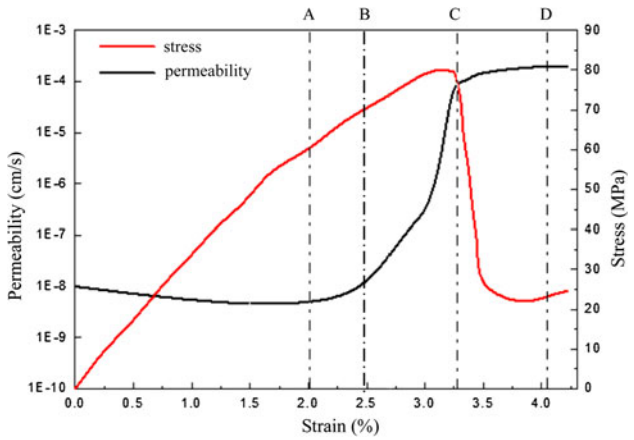

Fig. 4 Numerically obtained relationship among stress, permeability, and strain of the sample

1995; Pearce et al. 2000). The method is, mathematically, a linear and continuum mechanics method for numerically processing nonlinear and discontinuum mechanics problems in rock failure. With the advance in the performance of computers, an increasing number of researchers attempt to use the similar principle to solve discontinuous problems through continuum mechanics (Fang and Harrison 2002; Zhu and Tang 2004; Ma et al. 2011).

2.1.3 Permeability Variation of the Element with Damage

When an element of rock undergoes dilatancy due to the degradation of strength and stiffness, its hydraulic properties will change. Experimental results indicate that dilatancy leads to an increase in permeability. These changes in hydraulic properties can be directly related to either stress or strain (Stormont and Daemen 1992; Zhu and Wong 1997; Otto Schulze et al. 2001).

Most of the theories regarding stress-induced variations of permeability refer to the pre-failure phase. During elastic deformation, rock permeability decreases when the rock compacts and increases when the rock extends. The permeability variation for an intact rock element (when $D = 0$) in the elastic state can be described as (Louis 1974; Li and Wu 1997; Tang et al. 2002)

$$k_e = k_0 \exp[-\beta(\sigma_{ii}/3 - \alpha P)] \tag{15}$$

where k_0 is the initial permeability of the rock element, β is the coupling coefficient, and $\sigma_{ii}/3$ is the average total stress. In RFPA3D-Parallel, Eq. 15 is employed to represent the influence of stress on permeability for an intact rock element.

In the post-peak stage, rock elements undergo both instantaneous strength degradation and volumetric expansion. Although many experiments have shown that there is a clear correlation between volumetric dilatancy and the increase in permeability in brittle rocks at the micro-scale, it is generally difficult to characterise small-scale elements accurately and then relate their properties to macroscopic

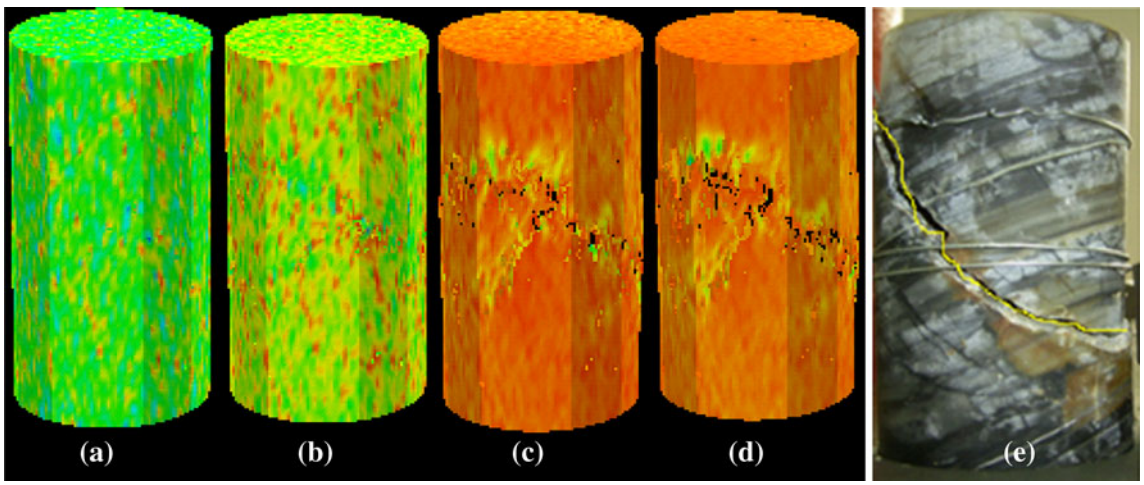

Fig. 5 Failure process of sample: **a**–**d** numerical results; **e** experimental result

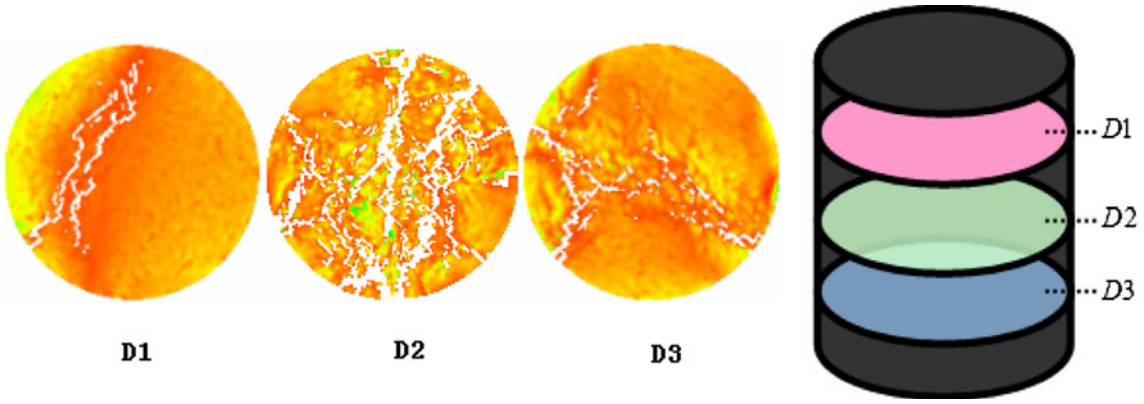

Fig. 6 Fracture pattern at different section in the sample

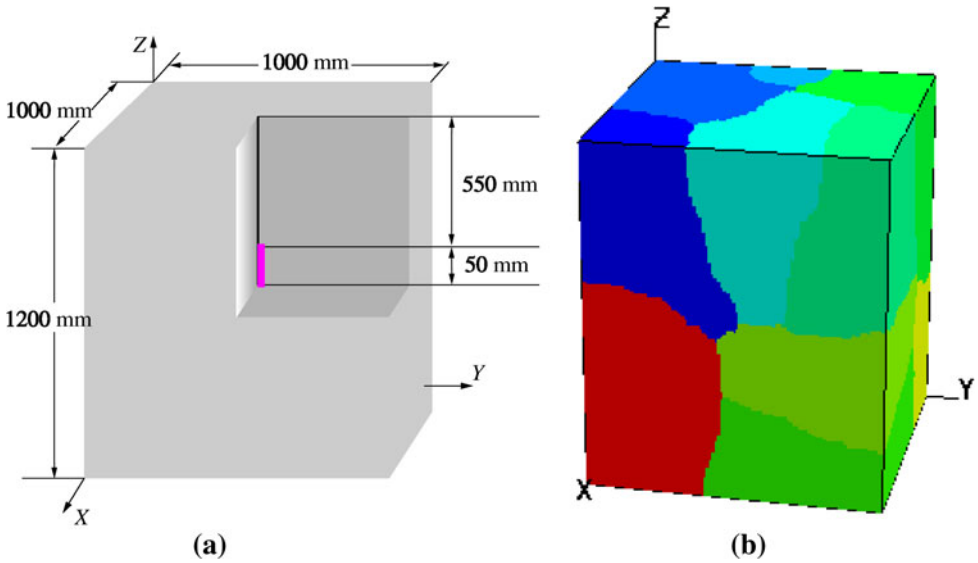

Fig. 7 Model configuration: **a** model geometry, **b** 12 sub-domains for parallel FEM computation

Table 2 Confining pressures

Case	σ_x (MPa)	σ_y (MPa)	σ_z (MPa)
I	4.0	4.0	1.0
II	1.0	3.0	5.0
III	1.0	1.0	1.0

Table 3 Rock properties

Parameters	Value	Unit
Homogeneity index (m)	4.0	
Young's modulus (E_0)	6	GPa
Compressive strength (f_c)	100	MPa
Poisson's ratio (v)	0.25	
Internal friction angle (ϕ)	30	°
Uniaxial tensional strength (f_t)	10	MPa
Permeability coefficient (k_0)	1e−5	cm/s
Coefficient of pore-water pressure (α)	0.8	
Coupling coefficient (β)	0.01	

hydraulic properties that are of practical interest (Shao et al. 2005; Jaeger et al. 2007). In the FSD model, all the constitutive laws are based on a single mesoscopic element. This degradation is physically manifested as the development of fractures, and this is one of the important concepts addressed in the improved FSD model used in RFPA3D-Parallel. To apply appropriate post-peak hydraulic characteristics, the use of a strain-based formulation for the permeability variation may be more suitable (Susan et al. 2003; Yuan and Harrison 2005; Chen et al. 2007). On the basis of characterisation of deformation-dependent permeability proposed by Yuan and Harrison (2005), we assume that a damaged rock element may be represented hydraulically as a volume of rock containing three orthogonal fractures. This representation is shown conceptually in Fig. 2. Assuming that the three fractures are

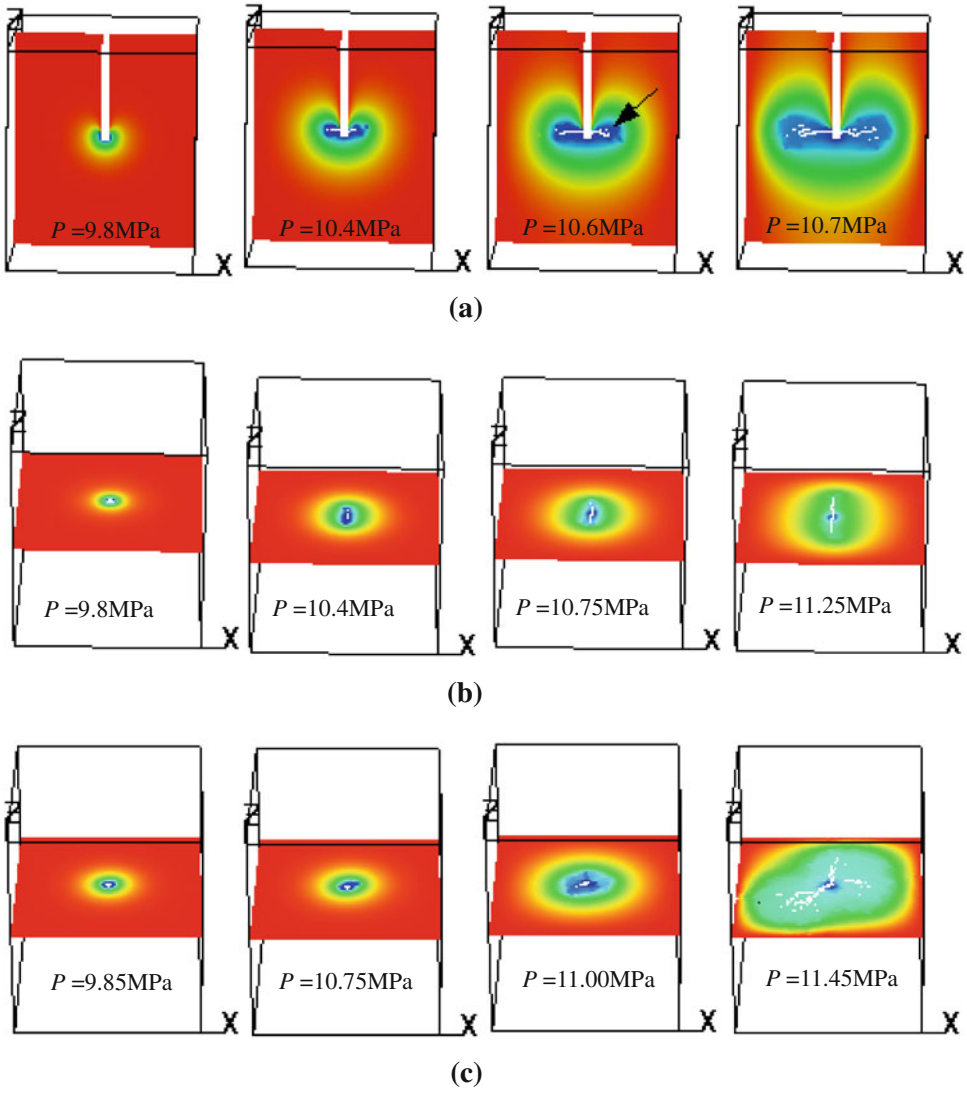

Fig. 8 Hydraulic fracturing process of case I, II and III. **a** Hydraulic fracturing mode of case I. **b** Hydraulic fracturing mode of case II. **c** Hydraulic fracturing mode of case III

planar and have parallel sides, the aperture of the fractures is given approximately by

$$d \approx \frac{\Delta V}{3l^2} \approx \frac{\varepsilon_v V}{3\sqrt[3]{V^2}} = \frac{\varepsilon_v \sqrt[3]{V}}{3} \tag{16}$$

where ΔV is the volume change of the element due to dilatation, and l is the side length of the element before dilatation. The so-called cubic law gives the flow rate between smooth parallel plates as

$$q = \frac{d^3 \rho_l g}{12\mu_l} \frac{\Delta H}{l} \tag{17}$$

where ΔH is the fluid (water) head loss across the two ends. In Eq. 17, the hydraulic conductivity is given by the term $d^2\rho_l g/12\mu_l$. Therefore, the hydraulic conductivity for a damaged rock element (when $D > 0$) can be expressed as

$$k_d = \frac{d^2 \rho_l g}{12\mu_l} = \frac{\sqrt[3]{V^2}\rho_l g}{108\mu_l} \varepsilon_v^2 \tag{18}$$

In RFPA3D-Parallel, Eq. 18 is employed to represent the permeability variation for a damaged rock element.

The model we have adopted for the permeability of a damaged (i.e. fractured) element is scale dependent; therefore, the mesh dependency in the RFPA3D simulation is unavoidable. To examine the mesh effect associated with the FSD model, we consider two points. One is to investigate the mesh effect associated with producing model results; the other is to identify the optimal mesh size with respect to the problem geometry. By incorporating the parallel FEM technique, enough elements are provided for minimising the mesh effect in the modelling of a certain problems needed to be solved.

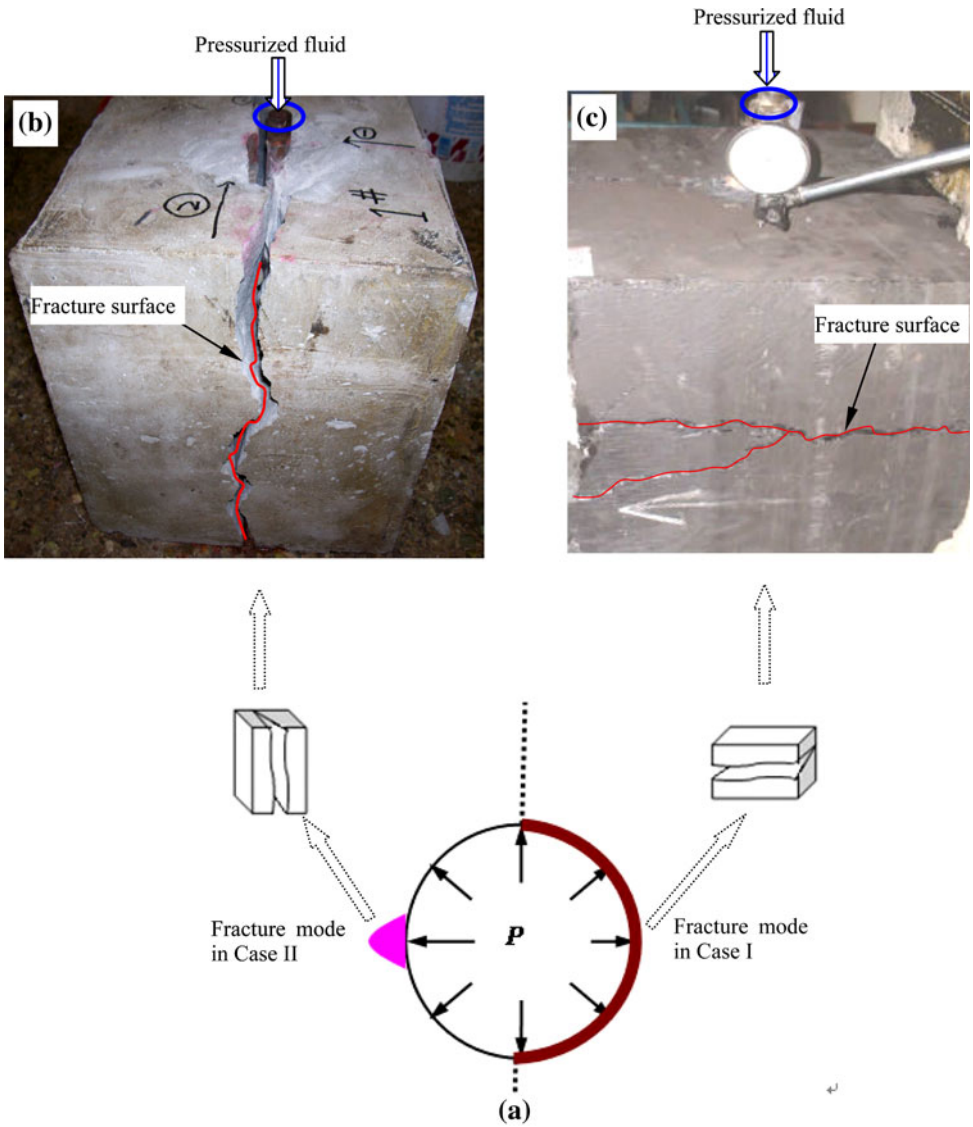

Fig. 9 Sketch of the effect of stress state on fracture mode: **a** the typical mode of fractures initiated from wellbore (Economides and Nolte 2000), **b** fracture parallel to wellbore (Meng et al. 2010), and **c** fracture perpendicular to wellbore (Deng et al. 2004)

2.2 Numerical Solution

In RFPA3D-Parallel, we rely on a parallel FEM to perform the seepage and stress analysis of the model by incorporating the message-passing interface (MPI) library. A cross-platform with seamless system integration between a Windows PC and a Linux HPC cluster is employed. The Windows PC works as a client, and the Linux HPC cluster serves as a server, offering finite element parallel computation. The pre/post processing parts and the failure analysis module utilise a user-friendly serial code running on Windows. The finite element computation, which consumes the most CPU resources and computation time, is parallelised on the Linux HPC cluster. The domain decomposition method (DDM), in which the physical domain is decomposed into many sub-domains, is adopted in the code. The number of sub-domains equals the number of processors involved in the calculation. To achieve load balance, each sub-domain has approximately the same number of elements. After partitioning, each sub-domain is assigned to one processor, and these processors will exchange data on the shared boundaries of the sub-domains. The data exchange is achieved by each processor sending messages to and receiving messages from processors with which it shares sub-domain boundaries. The number of shared boundaries should be as small as possible to minimise the communication cost. The parallel BICGSTAB (Bi-Conjugate Gradient Stabilised) iterative solver with a pre-conditioner is utilised to solve the system equations. BICGSTAB follows the algorithm described by Barrett et al. (1994) which makes it possible to solve the global equations by analysing these sub-domain stiffness

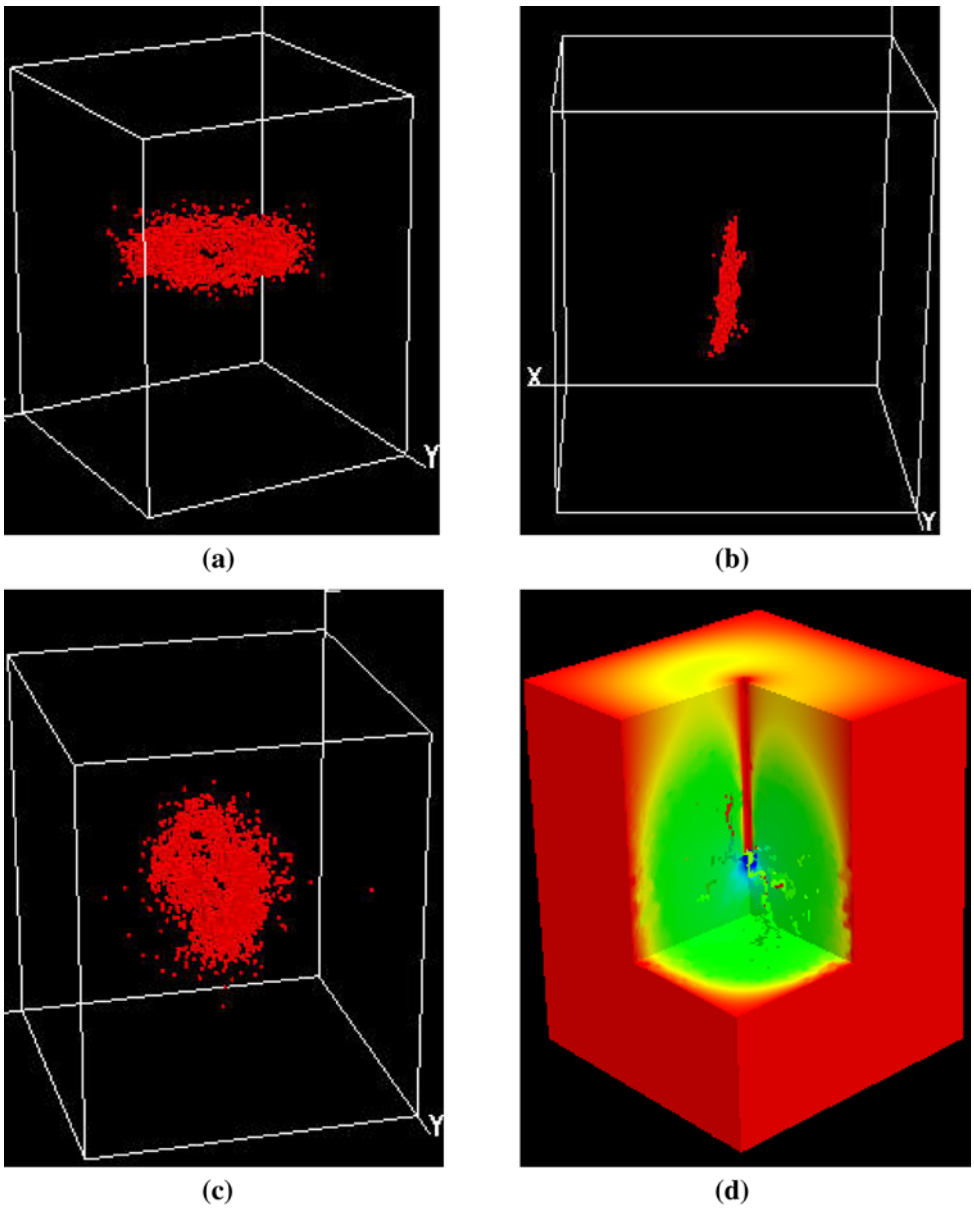

Fig. 10 Spatial distribution of fractures: **a** case I, **b** case II, **c** case III, and **d** case III-fracture mode in the section planes cutting through well bore

independently. This solver is highly efficient, scalable, and is able to solve large-scale FE equations. The parallel code is developed with Fortran 90 and C++ and is compiled with Intel Compilers. During the modelling, the stress field is examined, and elements strained beyond the pre-defined strength threshold level are assumed to be damaged irreversibly. The stiffness and strength of a damaged element will be reduced whereas its permeability will be increased accordingly. The model will then be re-analysed with the new parameters. The number of failed elements and the associated energy released, which can be treated as indicators of the acoustic emission (AE) activities accompanying rock failure, are also numerically simulated (Tang 1997).

3 Numerical Simulation of 3D Fracture Mode of Rock Specimen

To verify the accuracy of the improved FSD model and the capability of RFPA3D-Parallel, we simulated a three-dimensional cylindrical specimen with that was 45 mm in length and 20 mm in diameter. In the simulation with RFPA3D-Parallel, a generated crack has the width of an element. To reflect realistically the crack propagation in a rock sample, a large number of elements are necessary in the simulation (Aliabadi 1999). The cylindrical specimen is discretised into 680,000 elements and divided into 16 subdomains for parallel FEM computation on the HPC cluster. Constant upstream and downstream fluid pressures of 3.5

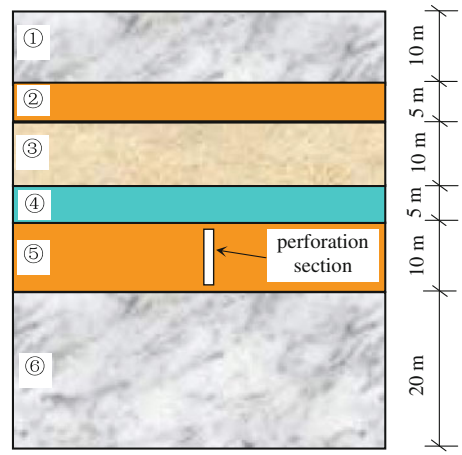

(a)

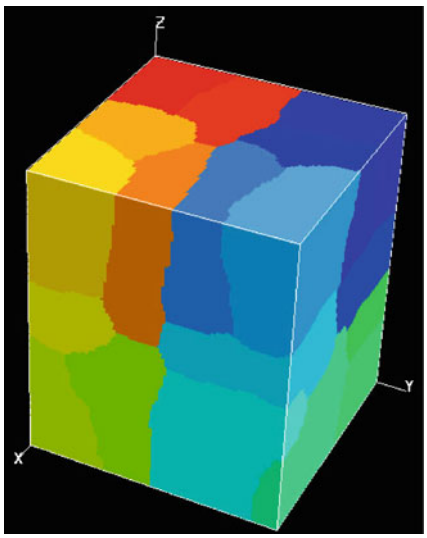

(b)

Fig. 11 Model configuration: **a** model geometry, **b** 24 sub-domains for parallel FEM computation

and 1.5 MPa, respectively, are applied to the bottom and top of the sample as shown in Fig. 3.

We numerically compress this sample vertically to simulate damage. The input parameters are reported in Table 1. Figure 4 shows the numerically obtained relationships between stress–strain and permeability variation. Figure 5 shows the numerically simulated progressive failure process. The simulation results compare well with experimental result (Fig. 5e). Initially, deformation is elastic, and permeability appears to decrease with compressive loading. As the axial strain increases to stage B, localised degradation (representing the onset of microcracking) begins to occur as specific elements attain their peak strengths. In stage A–B, these isolated flaws propagate, as expected, in the direction parallel to the maximum principal stress. This effect has been observed in numerous well-documented laboratory tests. In stage B–C, the permeability increases until yielding, leading to a significant increase in permeability. Therefore, the permeability increase is due to the microfractures connected by isolated flaws within the sample. In other words, the macroscopic flow behaviour depends not only on local permeability variations but also on the connectivity of the more conductive elements.

Figure 6 is the final fracture mode in a different section of the simulation. One can clearly observe the crack configurations, including the length, angle and density. In sections D1 and D3, the number of macrofractures is limited, while both macrofractures and isolated flaws (microfractures) are very abundant where section D2 intersects the primary fracture surface.

4 3D Numerical Simulation of Hydraulic Fracturing Process

4.1 Hydraulic Fracturing Behaviour at Different Confining Pressures

The success or failure of hydraulic fracturing technology is largely dependent on the design of fracture configurations and the optimisation of treatments compatible with the in situ conditions of a given reservoir. The in situ stress is the primary factor in determining the orientation of propagating hydraulic fractures. A small-scale model is used to investigate the behaviour of the fracturing away from the wellbore under different stress regimes, as shown in Fig. 7.

Table 4 Physico-mechanical parameters for case I

Rock layer	Young's modulus E_0/GPa	Compressive strength f_c/MPa	Tensile strength f_t/MPa	Internal cohesive angle ϕ/(°)	Poisson's ratio v	Density ρ/(kN m^{-3})	Hydraulic conductivity k_0/(cm s^{-1})	Coefficient of pore-water pressure (α)
①	40	100	10	35	0.20	26	1e−7	0.9
②, ⑤	30	40	4	30	0.30	25	1e−5	0.9
③	25	35	3.5	30	0.30	25	1e−7	0.9
④	15	30	3	30	0.30	25	1e−7	0.9
⑥	30	60	6	30	0.25	26	1e−7	0.9

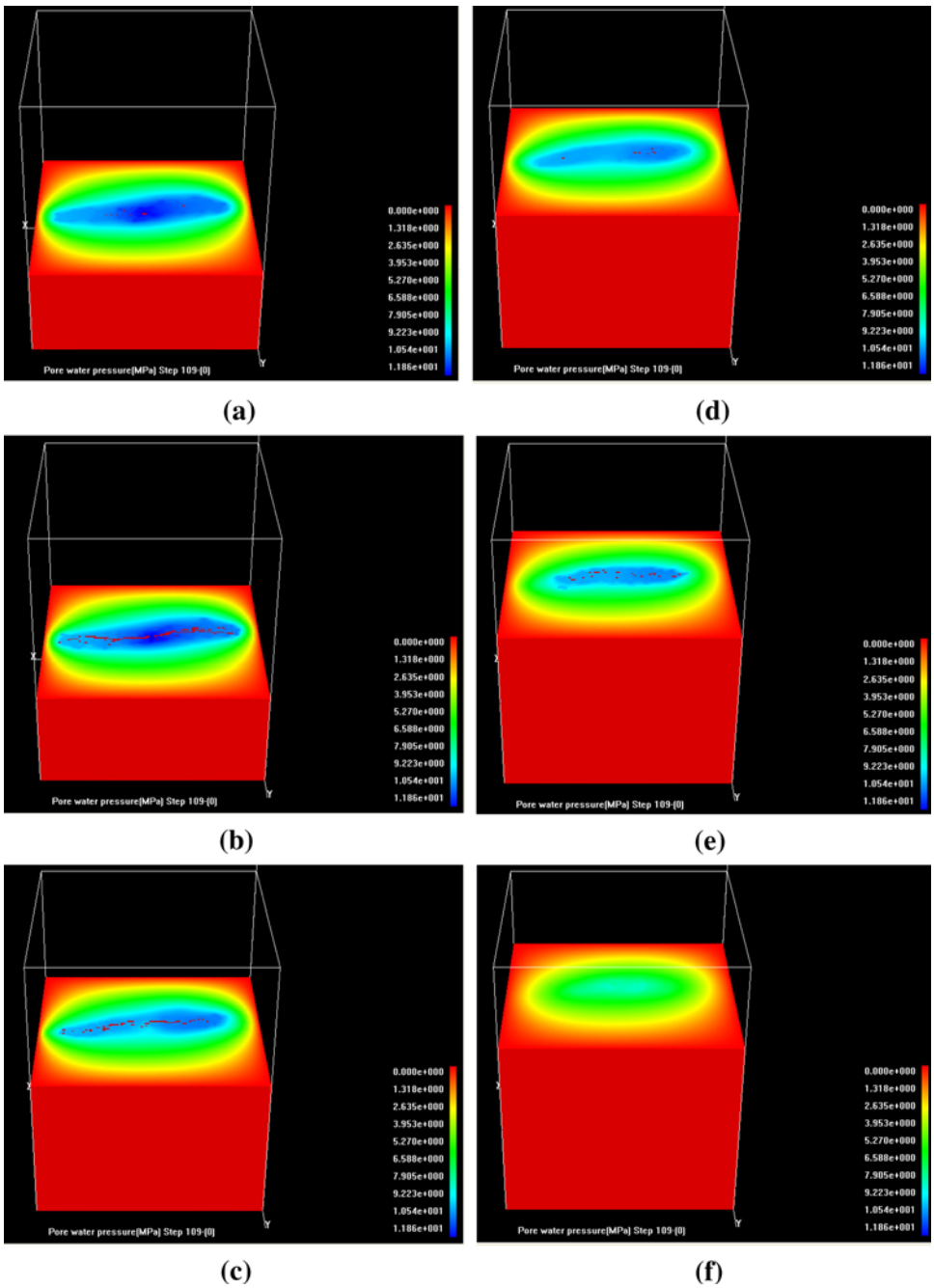

Fig. 12 Configuration of hydraulic fractures for case I at different section along *Z*-axial. **a** $Z = 20$ m, **b** $Z = 25$ m, **c** $Z = 30$ m, **d** $Z = 32$ m, **e** $Z = 35$ m, **f** $Z = 45$ m

A wellbore with a diameter of 40 mm is assumed to be located at the centre of a 1,000 mm × 1,000 mm × 1,200 mm block. The block was discretised into 1,200,000 elements (100 × 100 × 120) and 12 sub-domains for parallel FEM computation on the HPC cluster. A perforated section (which is subjected to hydraulic pressure) is located in the centre of the wellbore. Hydraulic pressure is applied along the boundary of the interior hole in the perforated section at an initial pressure of 8.5 MPa. The rate of pressurisation increase is kept constant throughout the numerical tests at 0.05 MPa/step.

It is assumed that the fluid is Newtonian and that the rock formation is permeable. Three different cases are simulated to illustrate the influence of the far-field stress on the hydraulic fracturing behaviour. The applied confining stresses, representing the effect of the far-field stresses, are reported in Table 2, and the borehole axis is aligned with one of the in situ stress directions. The mechanical parameters used in the modelling are reported in Table 3.

Figure 8a shows the evolution of pore pressure during the hydraulic fracturing process for case I (at section $X = 500$ mm). Generally, there is no preferential location

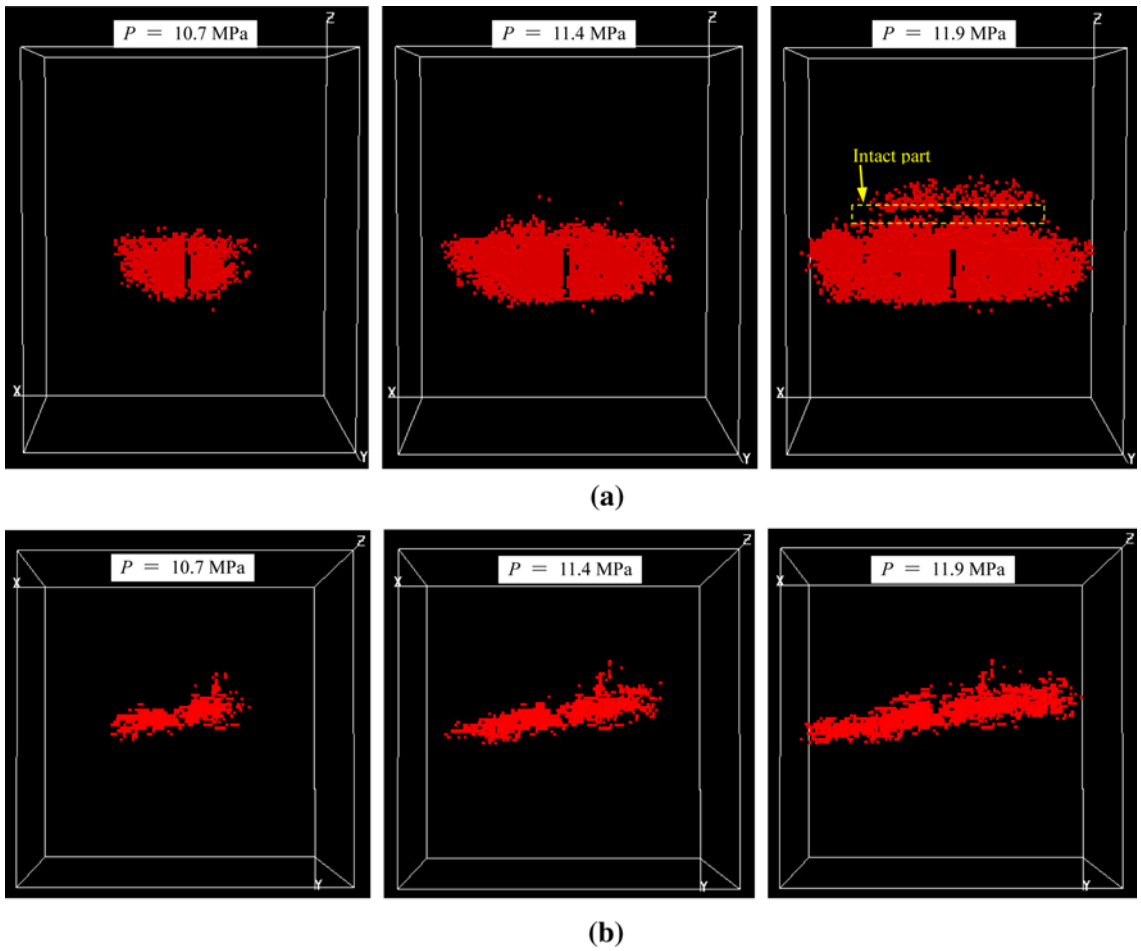

Fig. 13 Numerically obtained hydraulic fracturing mode of case I: **a** side view in Y–Z plane, and **b** overlooking view in X–Y plane

along the wellbore wall for the fracture to initiate because the geometry of the sample is symmetrical and the magnitudes of the far-field stresses σ_x and σ_y are equal. Therefore, the location and orientation of the fracture initiation is unpredictable. However, the macroscale orientation of the fractures is horizontal, i.e. the fractures formed in a plane perpendicular to the Z axis.

Figure 8b and c show the numerical results for cases II and III, respectively. The pressure for fracture initiation for all three cases is approximately 10 MPa, which is close to the theoretical value based on elasticity, although there is a small error induced by the heterogeneity of the materials. On the basis of the numerical results, one can conclude that the propagation of the hydraulic fractures is controlled by the far-field stress orientation. The hydraulic fracture selects the path of least resistance through the material, and the random locations of the individual heterogeneities result in an irregular hydraulic fracture trajectory. In reality, a perfect transverse fracture (i.e. a perfectly planar fracture perpendicular to any stress direction) is not possible in highly heterogeneous reservoir rock.

As soon as the fracture propagates slightly out of plane, the shear stress component reorients the fracture towards the preferred direction for fracture propagation with minimum resistance. For example, although the cracks in case I and II initiated and propagated in a plane, they branched out after growing for a short distance. Isolated fractures also open within the rock mass. Such fractures generate from weak elements. Despite these fractures, cases I and II represent two typical fracture modes in hydraulic fracturing process, as shown in Fig. 9. The numerically obtained fracture pattern closely resembles experimentally observed hydraulic fracture paths (Meng et al. 2010; Deng et al. 2004).

Case III shows multiple major fracture traces that are formed without any preferred orientations. The traces show significant branching and isolated fracturing. Because the magnitudes of the far-field stress in x, y, and z direction are identical to each other, the crack pattern in this case depends completely on the local homogeneity. Much of the energy from the hydraulic pressure was consumed by the branching of the fractures. Detournay and Carbonell (1994)

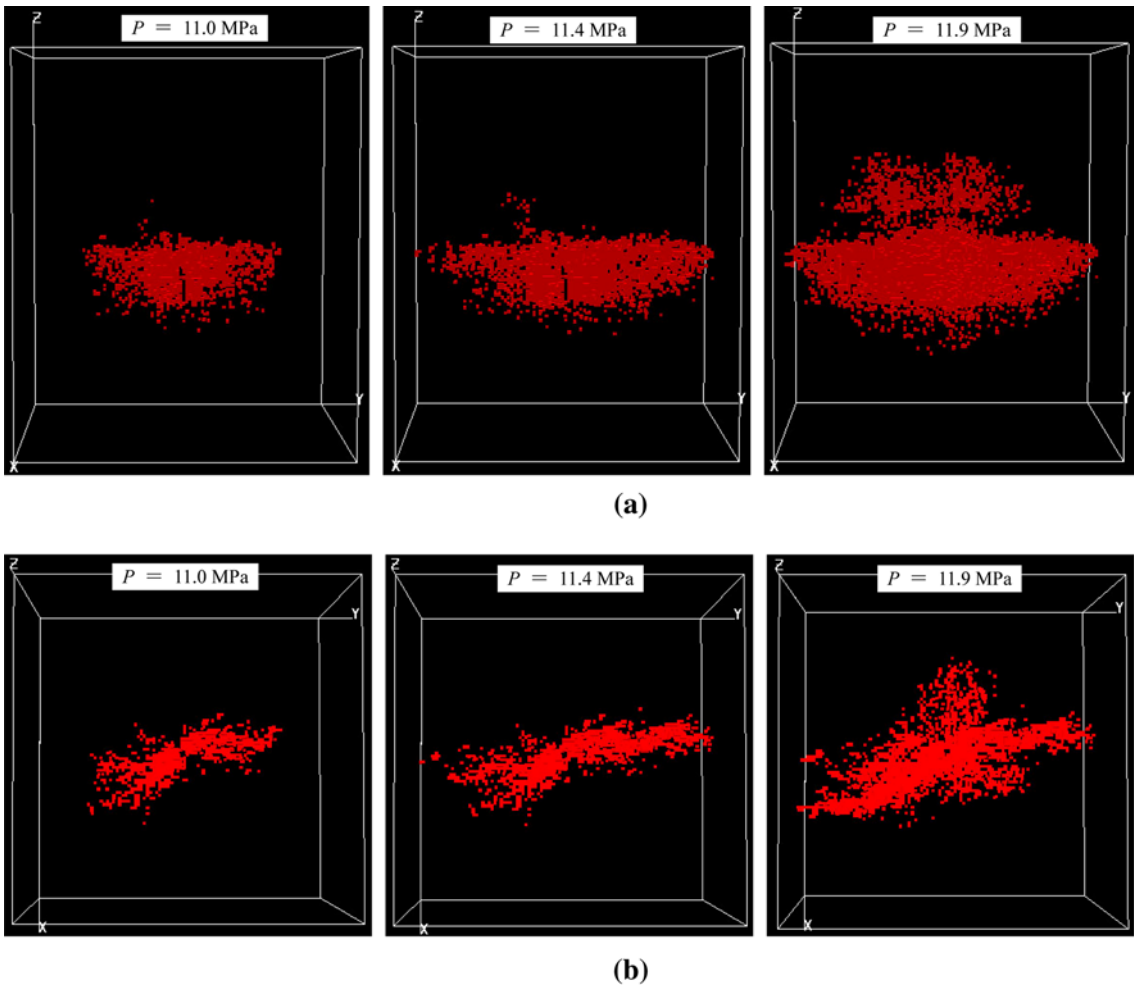

Fig. 14 Numerically obtained hydraulic fracturing mode of case II: **a** side view in Y–Z plane, and **b** overlooking view in X–Y plane

noted that fractures always propagate unstably at slow pressurisation rates and uniform far-field stress conditions. The breakdown pressures for cases I, II, and III are 10.7, 11.25, and 11.45 MPa, respectively. The greater the difference in the magnitude of the far-field stresses, the lower the hydraulic pressure for the propagation of fractures will be.

Figure 10 shows the corresponding fracture modes for the three cases. The visualisation of complex fracture growth along the non-preferred direction illustrates the physical phenomena that lead to increasing injection pressure and decreasing fracture volume.

4.2 Hydraulic Fracturing Behaviour in Multiple Rock Layers

Fluid-driven or hydraulic fractures, either natural or man-made, that propagate vertically in horizontally layered rocks may interact with interfaces and intersect different layers. To illustrate the complexity and the challenges involved in modelling hydraulic fractures in multi-layer strata, a conceptual model is employed, as shown in Fig. 11. The model contains six rock layers with varying stiffnesses and permeabilities, and the interfaces between the layers are assumed to be perfectly bonded. Layer No. 2 and No. 5 are assumed to be pay zone layers, and the lower pay zone layer (No. 5) is selected to be hydraulically fractured. An 8-m-high perforated section is located in the centre of layer No. 5. Hydraulic pressure is applied along the boundary of the interior hole in the perforated section. Initial stresses of $\sigma_x = 5.0$ MPa, $\sigma_y = 5.0$ MPa, and $\sigma_z = 10.0$ MPa are applied on the outer boundaries of the model. The model has been discretised into 1,200,000 elements ($100 \times 100 \times 120$) and 24 sub-domains for parallel FEM computation on the HPC cluster. The physico-mechanical parameters employed in the calculation are reported in Table 4. To investigate the effect of the rock strata properties on the fracturing mode, another two cases (cases II and III) were considered. In case II, the elastic modulus and strength properties are assumed to be reduced

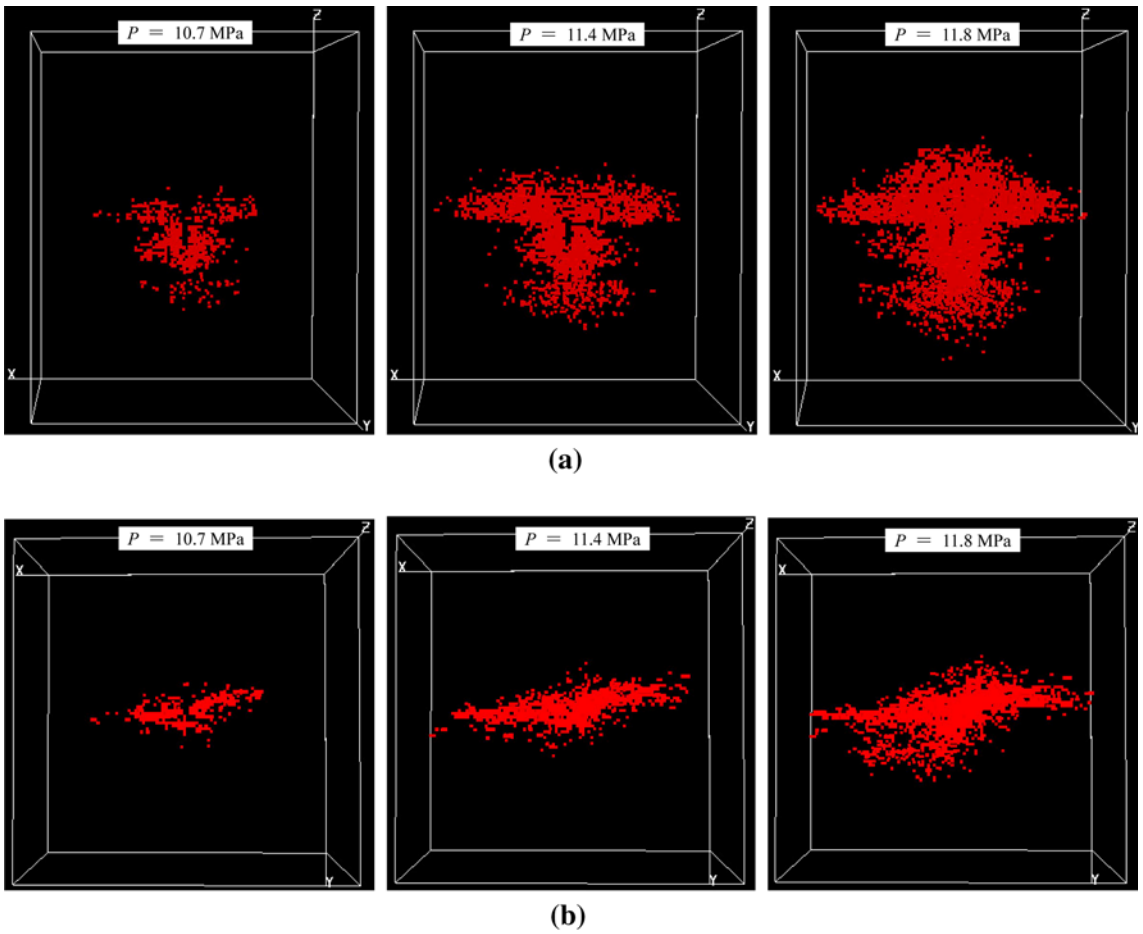

Fig. 15 Numerically obtained hydraulic fracturing mode of case III: **a** side view in Y–Z plane, and **b** overlooking view in X–Y plane

by 10 %, compared with those of case I, while in case III, the elastic modulus and strength properties are reduced by 20 %, compared with those of case I. The other parameters were kept constant in cases II and III.

The numerically simulated fracturing mode is shown in Fig. 12, and the corresponding fracturing mode is shown in multiple views in Fig. 13. The pressure gradient is increased for a relatively narrow fracture channel that carries the relatively high flow rate. The initiation and propagation of fractures are generally restricted within the pay zone layer, although a few isolated short fractures (flaws) appear in the covering layer. One should note that there is an intact layer between the pay zone layer and the covering layer, which indicates that the fracture in the pay zone layer did not propagate into the covering layer. The randomly distributed short fractures in the covering layer are formed within the weakest elements, where the local tensile stress reaches the local tensile strength. The tensile stress results mainly from the local pore pressure (the rock formation is assumed to be permeable) and the contrasts in the elastic properties of the involved strata. Therefore, the arrangement of these isolated short fractures is concordant with the direction of the macrofracture in the pay zone layer. As such, only a primary fracture, and no distinct fracture branches and offsets, forms in the pay zone layer.

Figures 14 and 15 show the fracturing modes for case II and case III, respectively. The fluid-driven fractures clearly propagate across the interfaces from the pay zone layer to adjacent layers and continue to propagate. By overcoming the higher vertical stress and the extra compressive stress generated from the interaction between the fractures, each fracture is initiated in a non-preferred direction, turns and twists during propagation, and tends to align itself with the preferred direction and plane. Of all three cases, the results from case III are the most disappointing because the length of the fracture in the pay zone layer is short while most of fractures propagate into the adjacent layers.

The results indicate that the material properties, Young's modulus and strength can influence fracture propagation. According to the elasticity considerations applied to perfectly bonded interfaces or strong interfaces, a fracture that initiates in the stiffer of the two layers is able to advance towards and enter the softer layer but is not able to grow from the soft layer to the stiff layer (Erdogan and

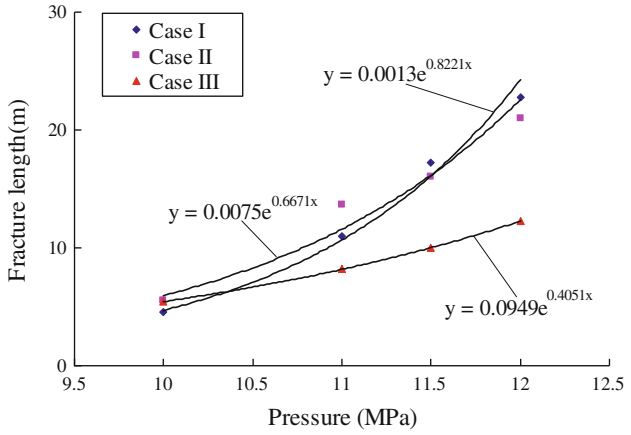

Fig. 16 Relationship between the magnitude of hydraulic pressure and length of fracture in pay zone layer

Biricikoglu 1973; Helgeson and Aydin 1991; Zhang et al. 2007). If the adjacent layer has a higher Young's modulus than that of the layer with the fracture, the strain energy decreases as the fracture tip approaches the interface, and propagation will be impeded. For the opposite case, the strain energy will be enhanced, and the fracture continues to propagate across the interface and into the intact adjacent layer. Compared with case I, stronger adjacent rock layers with higher toughness are found to efficiently resist fracture propagation from the pay zone layers.

Since the stress barrier near the interface is weak because of the flexibility of the intact soft layer, the local heterogeneity is more likely to induce out-of-plane fracture growth (Mofazzal Hossain and Rahman 2008). In reality, the rock formation in the field is extremely heterogeneous. The variation in failure mode is highly sensitive to the local features of the rock mass. As a result, the fracture surface is rough, and mixed-mode fracture propagation further affects the non-planar fracture growth in the non-preferred direction. In reality, there are two types of failure, high-stress failure and low-strength failure, for different materials. In a homogeneous material, failure begins at the high-stress site whereas, in a heterogeneous material (e.g. rock), failure may start at the weaker locations because of the presence of pores, microfractures, and grain boundaries. This observation led Fairhurst (1964) to introduce the notion of "stress severity", which represents the ratio of the theoretical stress at the moment of failure to the stress that would theoretically be necessary for failure at any given point. Heterogeneity is the main reason for failures that occur in locations where the stress is not necessarily the greatest.

Figure 16 shows the relationship between the magnitude of hydraulic pressure and the length of the fracture in the pay zone layer. In case III, a higher pressure is required for the fracture to reach the same length as those in cases I and II. Once branches and offsets appear during the hydraulic fracturing process, the fractures that develop such offsets in their path require high fluid pressure to sustain fracture growth, as was suggested by previous studies (Medlin and Fitch 1983; Mofazzal Hossain and Rahman 2008; Zhang et al. 2008). Regardless of what generates the multiple fractures and what causes them to turn and twist during propagation, they are the source of high treating pressures and reduced fracture volume. These characteristics have clearly been simulated in the small-scale models examined in this study. The results indicate that complex fracture growth in non-preferred directions is the most likely reason for premature screen-outs in many fracture treatments in the field. In addition, the resulting reduced fracture volume is a major reason for reduced productivity from the fractures.

5 Conclusions

In this study, a parallel finite element program, RFPA3D-Parallel, is developed with MPI and employed for stress and seepage fluid field analysis. The constitutive law of this model considers strength and stiffness degradation, stress-dependent permeability for the pre-peak stage, and deformation-dependent permeability for the post-peak stage. The hydraulic fracturing process inside a rock specimen is numerically simulated using this model. Three coupled processes are considered: (1) mechanical deformation of the solid medium that is induced by the fluid pressure acting on the fracture surfaces and the rock skeleton, (2) flow of fluid within the fracture, and (3) propagation of the fracture.

3D modelling of progressive failure and associated fluid flow in heterogeneous rocks was used to investigate the hydro-mechanical response of the rock specimen at the scale of typical laboratory samples. The responses investigated include the axial stress–axial strain and the associated permeability evolution, as well as the fracture patterns that develop at various stages of loading. The simulation results compare well with previous experimental results. The results show that RFPA3D-Parallel can accurately analyse coupled fluid flow and deformation, which is necessary to model the fluid-driven propagation of hydraulic fractures.

The 3D modelling of the hydraulic fracturing process was conducted on HPC clusters. In the case of a large difference in the magnitude of the far-field stresses, a fracture from a vertical wellbore will propagate along the maximum stress direction without branching, turning and twisting. In other cases, the fracture often initiates in a non-preferred direction then turns and twists during propagation to align with the preferred direction and plane; such

fracturing especially occurs in rock formations that contain multiple layers with different material properties. These fractures have been successfully simulated in this study. The results show that the local heterogeneity of the rock matrix and the macro-scale stress fluctuations due to the variation in material constants are the major cause of the branching, turning, and twisting of fractures. Hydraulic fractures that develop such offsets require high fluid pressure to sustain fracture growth. These features are the source of the high treating pressures and reduced fracture volume.

Although natural cases are often much more complex than the numerical models considered here, the study highlights some interesting phenomena for complex 3D hydraulic fracturing in rock masses. Using the present model, many factors associated with hydraulic fracturing engineering will be considered in the future. For example, (a) many effects related to the modelling of proppant transport (e.g. the interaction and collision between proppant particles, shear-induced proppant migration, and proppant settling) will be considered; (b) non-Newtonian fluids will be considered in a future model; and (c) how to handle the residual deformation is one of the subjects of ongoing and future research concerning FSD model and RFPA3D-Parallel code.

Acknowledgments The authors would like to thank Prof. Giovanni Barla, Prof. Omer Aydan, and Dr. Corrado Fidelibus for their constructive comments on this paper. The study presented in this paper was jointly supported by grants from the National Basic Research Programme of China (Grant No. 2011CB013503) and the National Natural Science Foundation of China (Grant Nos. 51121005, 51079010, and 50909013). The work was also partially supported by ARC Australian Laureate Fellowship grant FL0992039 and ARC CoE Early Career Award grant CE110001009. The authors are grateful for these supports.

References

Abass HH, Saeed Hedayati, Meadows DL (1992) Halliburton services. Non-planar fracture propagation from a horizontal wellbore: experimental study. SPE 24823, pp 324–339

Adachi J, Siebrits E, Peirce A, Desroches J (2007) Computer simulation of hydraulic fractures. Int J Rock Mech Min Sci 44:739–757

Aliabadi MH (1999) Fracture of rock. Computational Mechanics Publications, WIT Press, Boston

Barree RD (1983) A practical numerical simulator for three-dimensional fracture propagation in heterogeneous media. SPE Paper No 12273

Barrett R, Berry M, Chan TF, Demmel J, Donato J, Dongarra J, Eijkhout V, Pozo R, Romine C, Vander Vorst H (1994) Templates for the solution of linear systems: Building blocks for iterative methods. Society for Industrial Mathematics, Philadelphia

Biot MA (1941) General theory of three-dimensional consolidation. J Appl Phys 12:155–164

Blaheta R, Byczanski P, Jakl O, Kohut R, Kolcun A, Krecmer K, Stary J (2006) Large-scale parallel FEM computations of far/near stress field changes in rocks. Future Gener Comput Syst 22:449–459

Carter BJ, Desroches J, Ingraffea AR, Wawrzynek PA (2000) Simulating fully 3D hydraulic fracturing. In: Zaman M, Booker J, Gioda G (eds) Modeling in geomechanics. Wiley Publishers, New York

Chen YF, Zhou CB, Sheng YQ (2007) Formulation of strain-dependent hydraulic conductivity for a fractured rock mass. Int J Rock Mech Min Sci 44:981–996

Crosby DG, Yang Z, Rahman SS (1998) The successful use of transverse hydraulic fractures from horizontal wellbores. SPE 50423, pp 128–136

Deng GZ, Wang SB, Huang BX (2004) Research on behavior character of crack development induced by hydraulic fracturing in coal-rockmass. Chin J Rock Mech Rock Eng 23(20):3489–3493

Detournay E, Carbonell R. (1994) Fracture mechanics analysis of breakdown process in minifrac or leak-off tests. In: Proc, Eurock'94, Balkema, Rotterdam, pp 399–407

Dong CY, de Pater CJ (2001) Numerical implementation of displacement discontinuity method and its application in hydraulic fracturing. Comput Methods Appl Mech Eng 191:745–760

Economides MJ, Nolte KG (2000) Reservoir stimulation. Wiley, Singapore

Erdogan F, Biricikoglu V (1973) Two bonded half planes with a fracture going through the interface. Int J Eng Sci 11:745–766

Fairhurst C (1964) On the validity of the Brazilian test for brittle materials. Int J Rock Mech Min Sci 1:535–546

Fang Z, Harrison JP (2002) Development of a local degradation approach to the modelling of brittle fracture in heterogeneous rocks. Int J Rock Mech Min Sci 39:443–457

Garcia JG, Teufel LW (2005) Numerical simulation of fully coupled fluid-flow/geomechanical deformation in hydraulically fractured reservoirs. SPE Paper 94062, 2005 SPE Production and Operations Symposium, Oklahoma, USA

Geertsma J, de Klerk F (1969) A rapid method of predicting width and extent of hydraulically induced fractures. J Pet Tech 21:1571–1581

Helgeson DE, Aydin A (1991) Characteristics of joint propagation across layer interfaces in sedimentary rocks. J Struct Geol 13:897–911

Jaeger JC, Cook NGW, Zimmerman RW (2007) Fundamentals of rock mechanics, 4th edn. Blackwell, Oxford

Khristianovic SA, Zheltov YP (1955) Formation of vertical fractures by means of highly viscous liquid. In: Proceedings of the fourth world petroleum congress, Rome, pp 579–586

Lee SH, Ghassemi A (2011) Poroelastic rock failure analysis around multiple hydraulic fractures using a BEM/FEM model. In: 45th US rock mechanics/geomechanics symposium held in San Francisco, USA

Legarth B, Huenges E, Zimmermann G (2005) Hydraulic fracturing in a sedimentary geothermal reservoir: results and implications. Int J Rock Mech Min Sci 42:1028–1041

Li SP, Wu DX (1997) Effect of confining pressure, pore pressure and specimen dimension on permeability of Yinzhuang sandstone. Int J Rock Mech Min Sci 34:435–441

Li LC, Tang CA, Tham LG, Yang TH, Wang SH (2005) Simulation of multiple hydraulic fracturing in non-uniform pore pressure field. Adv Mater Res 9:163–172

Li LC, Tang CA, Li CW, Zhu WC (2006) Slope stability analysis by SRM-based rock failure process analysis (RFPA). Geomech Geoeng Int J 1:51–62

Li LC, Yang TH, Liang ZZ, Tang CA (2011a) Numerical investigation of groundwater outbursts near faults in underground coal mines. Int J Coal Geol 85(3):276–288

Li LC, Tang CA, Wang SY (2011b) A numerical investigation of fracture infilling and spacing in layered rocks subjected to hydro-mechanical loading. Rock Mech Rock Eng. doi:10.1007/s00603-011-0194-x

Liang ZZ, Tang CA, Li HX, Xu T, Zhang YB (2004) Numerical simulation of 3-D failure process in heterogeneous rocks. Int J Rock Mech Min Sci 41:323–328

Louis C (1974) Rock hydraulics. In: Muller L (ed) Rock mechanics. Springer, Vienna

Ma GW, Wang XJ, Ren F (2011) Numerical simulation of compressive failure of heterogeneous rock-like materials using SPH method. Int J Rock Mech Min Sci 48:353–363

Mahrer KD (1999) A review and perspective on far-field hydraulic fracture geometry studies. J Pet Sci Eng 24:13–28

Medlin WL, Fitch JL (1983) Abnormal treating pressures in MHF treatments. In: SPE 12108, 58th SPE annual technical conference and exhibition, San Francisco, CA, USA

Meng QM, Zhang SC, Guo XM, Chen XH, Zhang Y (2010) A primary investigation on propagation mechanism for hydraulic fracture in glutenite formation. J Oil Gas Tech 32(4):119–123

Mofazzal Hossain Md, Rahman MK (2008) Numerical simulation of complex fracture growth during tight reservoir stimulation by hydraulic fracturing. J Pet Sci Eng 60:86–104

Nordren RP (1972) Propagation of a vertical hydraulic fracture. SPE J 12(8):306–314

Pearce CJ, Thavalingam A, Liao Z, Bicanic N (2000) Computational aspects of the discontinuous deformation analysis framework for modeling concrete fracture. Eng Fract Mech 65:283–298

Perkins TK, Kern LR (1961) Widths of hydraulic fractures. J Pet Tech 13(9):937–949

Pietruszczak S, Xu G (1995) Brittle response of concrete as a localization problem. Int J Solid Struct 32:1517–1533

Rungamornrat J, Wheeler MF, Mear ME (2005) A numerical technique for simulating nonplanar evolution of hydraulic fractures. In: SPE 96968, 2005 SPE annual technical conference and exhibition, Dallas, Texas, USA

Savitski AA, Detournay E (2002) Propagation of a penny-shaped fluid-driven fracture in an impermeable rock: asymptotic solutions. Int J Solids Struct 39:6311–6337

Schulze O, Popp T, Kern H (2001) Development of damage and permeability in deforming rock salt. Eng Geol 61:163–180

Shah KR, Carter BJ, Ingraffea AR (1997) Hydraulic fracturing simulation in parallel computing environments. Int J Rock Mech Min Sci 34:474–484

Shao JF, Zhou H, Chau KT (2005) Coupling between anisotropic damage and permeability variation in brittle rocks. Int J Numer Anal Meth Geomech 29:1231–1247

Siebrits E, Peirce AP (2002) An efficient multi-layer planar 3D fracture growth algorithm using a fixed mesh approach. Int J Numer Meth Eng 53:691–717

Simonson ER, Abou-Sayed AS, Clifton RJ (1978) Containment of massive hydraulic fractures. SPE J 18(1):27–32

Sousa JLS, Carter BJ, Ingraffea AR (1993) Numerical simulation of 3D hydraulic fracture using Newtonian and power-law fluids. Int J Rock Mech Min Sci Geomech Abstr 30:1265–1271

Stormont JC, Daemen JJK (1992) Laboratory study of gas permeability changes in rock salt during deformation. Int J Rock Mech Min Sci Geomech Abstr 29:325–342

Susan E, Minkoff C, Stone M, Bryant S (2003) Coupled fluid flow and geomechanical deformation modeling. J Pet Sci Eng 38:37–56

Tang CA (1997) Numerical simulation on progressive failure leading to collapse and associated seismicity. Int J Rock Mech Min Sci 34(2):249–261

Tang CA, Tham LG, Lee PKK, Yang TH, Li LC (2002) Coupled analysis of flow, stress and damage (FSD) in rock failure. Int J Rock Mech Min Sci 39(4):477–489

Vandamme L, Curran JH (1989) A three-dimensional hydraulic fracturing simulator. Int J Numer Meth Eng 28:909–927

Wang SY, Sun L, Au ASK, Yang TH, Tang CA (2009) 2D-numerical analysis of hydraulic fracturing in heterogeneous geo-materials. Constr Build Mater 23(6):2196–2206

Warpinski NR, Moschovidis ZA, Parker CD, Abou-Sajed IS (1993) Comparison study of hydraulic fracturing models: test case GRI-staged field experiment. SPE, pp 469–478

Yale DP, Lyons SL, Qin G (2000) Coupled geomechanics-fluid flow modeling in petroleum reservoirs: coupled versus uncoupled response. In: Girard J, Liebman M, Breed C, Doe T (eds) Pacific rocks 2000. Balkema, Rotterdam, pp 137–144

Yang TH, Tham LG, Tang CA, Liang ZZ, Tsui Y (2004) Influence of heterogeneity of mechanical properties on hydraulic fracturing in permeable rocks. Rock Mech Rock Eng 37(4):251–275

Yuan SC, Harrison JP (2005) Development of a hydro-mechanical local degradation approach and its application to modelling fluid flow during progressive fracturing of heterogeneous rocks. Int J Rock Mech Min Sci 42:961–984

Zhang X, Jeffrey RG (2006) The roles of secondary flaws and friction on deflection and reinitiation of hydraulic fractures at orthogonal preexisting fractures. Geophys J Int 166:1454–1465

Zhang X, Jeffrey RG, Thiercelin M (2007) Deflection and propagation of fluid-driven fractures at frictional bedding interfaces: a numerical investigation. J Struct Geol 29:396–410

Zhang X, Jeffrey RG, Thiercelin M (2008) Escape of fluid-driven fractures from frictional bedding interfaces: a numerical study. J Struct Geol 30:478–490

Zhu WC, Tang CA (2004) Micromechanical model for simulating the fracture process of rock. Rock Mech Rock Eng 37:25–56

Zhu WL, Wong TF (1997) The transition from brittle faulting to cataclastic flow: permeability evolution. J Geophys Res 102(B2):3027–3041